ELSEVIER

Journal of Nuclear Materials 220–222 (1995) 712–716

journal of nuclear materials

Edge plasma conditions and plasma–surface interactions in Extrap T1

H. Bergsåker, A. Möller, G.X. Li, G. Hellblom, J.H. Brzozowski, B. Emmoth, I. Gudowska

Royal Institute of Technology, Association Euratom-NFR, S-100 44 Stockholm, Sweden

Abstract

The T1 device is a toroidal machine with $R/a = 0.5$ m/0.06 m and stainless steel wall. It has been used to study high current density reversed field pinch plasmas. The edge plasma has been extensively investigated with double and triple Langmuir probes, heat flux probes and passive probes. Discharges with 40–90 kA plasma current is characterized by an edge density $n_e(a) \approx 10^{19}$ m^{-3}, $T_e(a) \approx 10$ eV and a high asymmetric parallel heat flux. A drift perpendicular to the magnetic field can be inferred from Langmuir probe measurements and passive probes and appears to be largely diamagnetic. Edge ion temperatures $T_i \geq 100$ eV are inferred from the saturation behaviour of hydrogen ions implanted in passive probes, from the high $q_{i\parallel}$ and from the inferred sputtering rate of metals.

1. Introduction

Extrap T1 is a toroidal machine with stainless steel walls, having a major radius $R = 0.5$ m and minor radius $a = 0.057$ m. It has been used to study the confinement properties of reversed field pinch discharges. As in other magnetic confinement schemes, the plasma performance is largely dependent on plasma–surface interactions, which are responsible for impurity production and hydrogen recycling and more generally establish boundary conditions for the plasma behaviour. Moreover, the integrity of the wall has been a concern in high power discharges.

To improve the understanding of plasma–surface interactions it is essential to study the edge plasma conditions. Quantities of interest are e.g. the edge electron temperature and density, the particle flux and heat flux, the edge ion temperature, electric fields and gradients of these. In T1 measurements on the edge plasma have been made with probes. We have reported previously on particle fluxes and impurity fluxes at the wall in 40 kA RFP discharges [1]. Data concerned with the edge ion temperature and perpendicular drift motion at the edge in 40 kA discharges have also been presented [2]. The studies were extended to plasma edge parameters in discharges with 40 and 90 kA plasma current [3]. In the present report we present edge profiles of relevant parameters in 40–90 kA discharges and attempt to draw some conclusions as regards plasma–surface interactions.

2. Experimental

The inner wall in T1 consists of six stainless steel bellows intersected by diagnostic and pumping port sections. Wall conditioning has been performed with dc glow discharge cleaning, moderate baking and pulse discharge cleaning with RFP discharges.

The inner radius of the bellows is 57 mm, the port sections carry fully poloidal constrictions at minor radius $r = 56$ mm and the diagnostic ports are 18 mm wide and are welded at $r = 59$ mm. Langmuir and passive probe measurements have been made using a probe manipulator which enters along the minor radius at 20° below the horizontal midplane, except for the passive probes in 40 kA shots when it entered at 20° above the midplane.

Probe heads as shown schematically in Fig. 1 have been used for active probes. For angularly resolved single and double Langmuir probe measurements, floating potential and calorimetric measurements a

0022-3115/95/$09.50
SSDI 0022-3115(94)00571-0

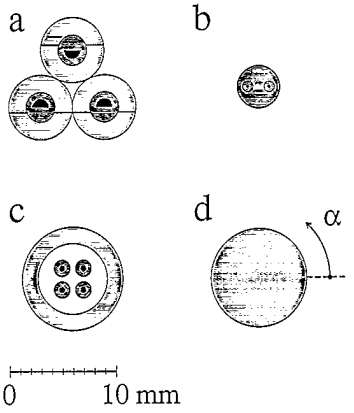

Fig. 1. A schematic view as seen from the plasma of the different probe heads which have been used. (a) A combined Langmuir and calorimetric probe array which can be rotated to measure at different angles with respect to the magnetic field. The three tungsten pins are partly shielded by surrounding graphite jackets. (b) A smaller double probe. (c) A four pin arrangement mainly for triple probe measurements. (d) A graphite cylinder exposed as a passive probe.

probe head has been employed which was used in Eta–Beta II [4]. It consists of three tungsten pins which are mounted in graphite protection in such a way that a pair of pins collects particles in one direction and a single pin in the opposite direction, all three at the same minor radius (Fig. 1a). Thermocouples are welded to the pins to measure the integrated heat deposition during a discharge. To sample current and heat flux in different directions the probe assembly was turned between discharges. The probe head shown in Fig. 1c is of a design which has previously been used on the TEXT tokamak [5], consists of four tungsten pins with stainless steel protection and is used for triple probe measurements.

The manipulator permits sample exchange between discharges and graphite cylinders with 9 mm radius have been exposed as passive probes to one or more complete discharges, with their flat front surface parallel to the inner wall (Fig. 1d). Following plasma exposure the cylinders were investigated with ion beam analysis methods.

The edge electron temperature was measured with Langmuir double or triple probe. To obtain double probe characteristics two procedures were adopted [3]. Either the current was measured throughout the discharge with constant applied bias, or the voltage was swept at 10 kHz. In the former case the average electron temperature had to be calculated from the average probe current in many similar discharges with different probe bias.

Measurements have been made in discharges with plasma current ranging from 40 to 90 kA and representative members of five different groups of shots are

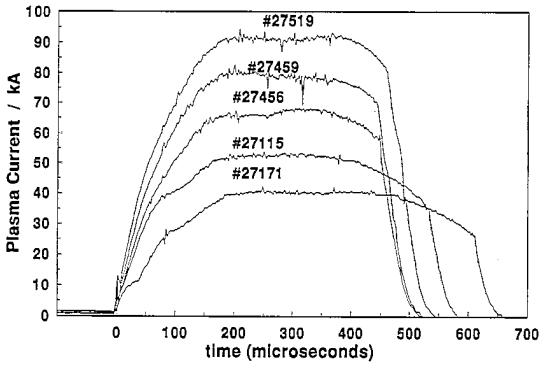

Fig. 2. Representative examples of 40, 50, 60, 75 and 90 kA discharges. The 40 and 50 kA discharges have $\theta \approx 2.1$ and the 60, 75 and 90 kA pulses have $\theta \approx 1.7$.

shown in Fig. 2. The pinch parameter θ is defied as the ratio $\theta = B_\theta(a)/\langle B_\varphi \rangle$ of edge poloidal field to average toroidal field. The discharges with nominally 40 and 50 kA current have $\theta \approx 2.1$, whereas the pulse with 60, 75 and 90 kA have $\theta \approx 1.7$. In the discharges considered here $\langle n_e \rangle = 1 \times 10^{20}$ m$^{-3} \pm 30\%$. The discharges with passive probe exposure were made in deuterium, whereas the active probe measurements were made in ordinary hydrogen.

3. Results

Fig. 3 shows the radial profiles of the parallel heat flux, averaged over a large number of complete discharges. The decay lengths are similar on electron and ion drift side, with $\lambda_q \approx 1.6$–2.2 mm in the high current discharges and $\lambda_q \approx 3.1$–3.8 mm in the low current shots. The heat flux is higher in the electron drift

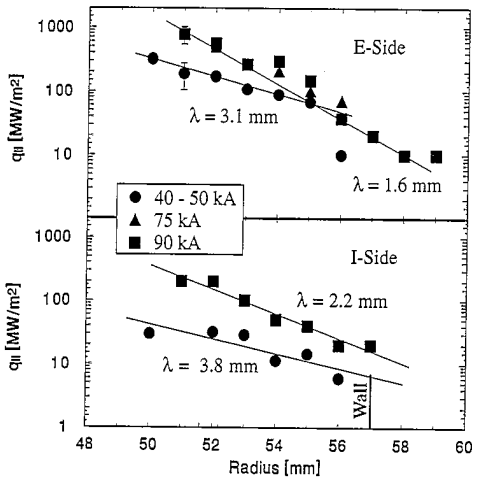

Fig. 3. Radial profiles of the parallel heat flux in electron and ion drift direction, averaged over many complete discharges.

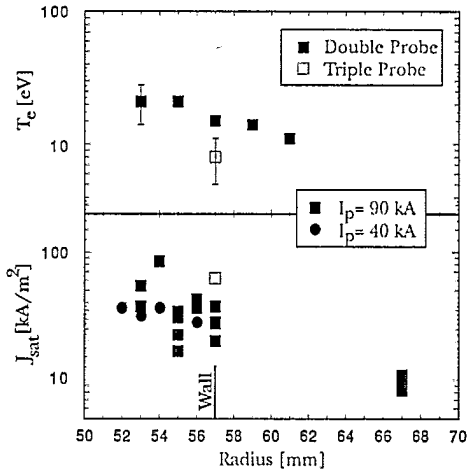

Fig. 4. Radial profiles of $T_e(r)$ and the ion saturation current density $j_{sat}(r)$. The double probe measurements are collected in the ion drift direction.

direction, by a factor 3 in the high current low θ shots and by a factor 6.5 in the low current high θ pulses.

Fig. 4 shows radial profiles of electron temperature and particle flux in the 90 kA discharges. These measurements are made with the probe of Fig. 1a facing the ion drift direction, and with the triple probe, which collects current in both directions. Fig. 5 shows the floating potential of the pins on the Fig. 1a probe in 90 kA discharges, in the electron and ion drift directions. The floating potential is ~5 V lower on the electron drift side. All these quantities are averaged over the time window 200–300 μs in many discharges.

Fig. 6 shows the buildup of deuterium and stainless steel on a graphite surface at wall position during exposure to 40 kA and 90 kA discharges. In the 40 kA

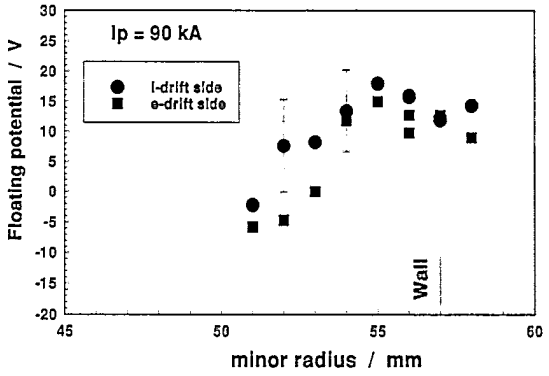

Fig. 5. The radial distributions in 90 kA discharges of the floating potential of the pins in the probe shown in Fig. 1a which face up and down (collecting flux in the ion- and electron drift directions respectively). Each point is an average over the time interval 200–300 μs in many discharges and the bars indicate shot to shot variation.

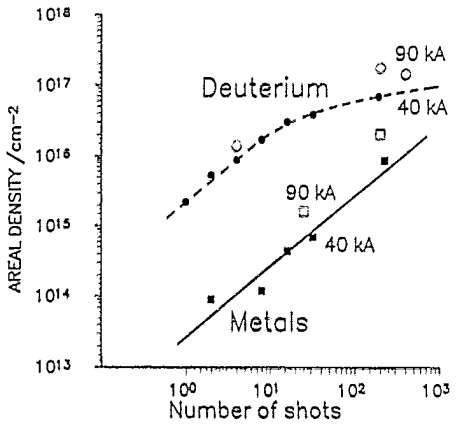

Fig. 6. Trapping of deuterium and collection of stainless steel components on graphite surfaces situated at the wall position ($r = 57$).

discharges, the trapping rate of deuterium at the wall position in short exposures, time averaged over complete discharges, was 4×10^{22} m^{-2} s^{-1}, and deuterium trapping saturated at 6×10^{20} m^{-2}. In the 90 kA discharges the corresponding numbers were found to be 6×10^{22} m^{-2} s^{-1} and 1.5×10^{21} m^{-2}, respectively. The collection rate of stainless steel components was 1–2% of the D trapping rate in the 40 kA discharges and roughly 3% in the 90 kA discharges.

Measurements were also made of angular distributions of the ion saturation current, turning the probe shown in Fig. 1a in different directions, and the trapping of deuterium and deposition of impurities on the cylindrical side of the graphite probes was measured as a function of the angle α which is indicated in Fig. 1d. A maximum current and deposition rate was consistently observed on the right hand side of the probes ($\alpha = 0$), as seen from the plasma. This asymmetry is illustrated with the examples in Fig. 7, where the flux ratio $R(\alpha) \equiv \Gamma(\alpha)/\Gamma(\alpha - \pi)$ is plotted in polar diagrams.

Following ~4000 RFP discharges there was a vacuum problem due to melting at a welding at one of the diagnostic ports. An endoscopic investigation was made of the vessel. Arc tracks and traces of melting could be seen, particularly at the diagnostic port sections and shell gaps. Qualitatively the damage around the ports could be correlated to the presence of remanent magnetisation at weldings and diagnostics equipment.

4. Discussion

An asymmetric heat flux at the edge, which is strongly peaked in the electron drift direction has been observed in other RFP experiments as well [4,6,7] and has been explained with a hot electron population

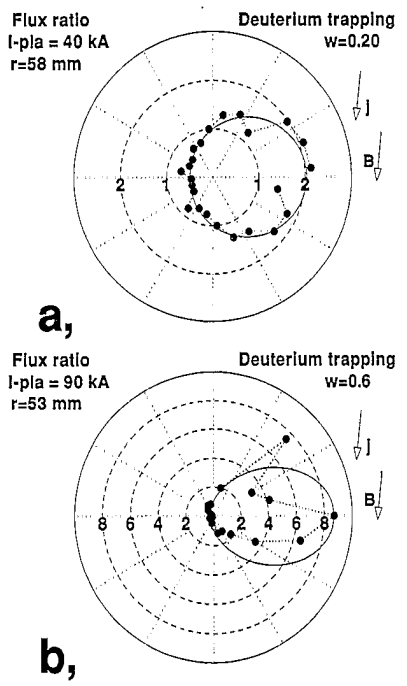

Fig. 7. Examples of asymmetric flux to the probes. The flux ratios $R(\alpha) \equiv \Gamma(\alpha)/\Gamma(\alpha - \pi)$ are plotted, where Γ is identified with of deuterium and metals on the cylindrical surface of the graphite probe shown in Fig. 1d.

escaping from the plasma core along stochastic field lines. That the heat flux in the electron drift direction is higher in high current, low θ discharges than in low current, high θ pulses has also been seen before [4] and can be understood within the framework of the kinetic dynamo theory [8]. In the present case the heat flux in the ion drift direction also increased with increasing plasma current.

The measured heat flux in the ion drift direction is indicative of high $T_i(a)$. It is customary to write the heat flux $q = \delta k T_e j_{sat}/e$, where the sheath energy transmission factor δ is a function of T_i/T_e [9]. For instance at $r = 53$ mm, with $j_{sat} = 80$ kA/m^2 and $kT_e = 27$ eV taken from Fig. 4, it will be necessary to use $\delta \approx 45$ to account for the 100 MW/m^{-2} heat flux, which corresponds to $T_i/T_e \approx 20$.

The floating potential in Fig. 5 is slightly lower on the electron drift side than on the ion drift side, possibly as a result of the suprathermal electron current, but the shape of the radial distribution $V_f(r)$ is similar. Using the electron temperature profile from Fig. 4 it is possible [9] to estimate the plasma potential V_p by $V_p \approx V_f + 3kT_e/e$. This gives an inward radial electric field of ~ 1.6 kV/m in the region $51 < r < 55$ and an outward field of ~ 4.5 kV/m for $55 < r < 58$ mm.

For deuterium to be trapped in graphite through monoenergetic ion implantation the energy has to be as high as ~ 350 eV to reach the areal density 6×10^{20} D/m^2 which was found in the 40 kA discharges [10,11]. To trap 1.5×10^{21} D/m^2 as in the 90 kA shots it is necessary to increase the implantation energy to ~ 1 keV. Clearly, with the edge electron temperatures around 10 eV, acceleration in the electrostatic sheath is insufficient to explain the trapping. If we consider the situation with high edge ion temperature, as indicated by the parallel heat flux, we may apply the fitting procedure recommended by Wampler [11] to derive the flux and energy of the incident particles. The dashed line in Fig. 6 shows the fit for the 40 kA case and corresponds to $kT_i = 105 \pm 10$ eV and an averaged radial flux $\Gamma_r \approx 7 \times 10^{22}$ D m^{-2} s^{-1}. By the same arguments, $\Gamma_r \approx 9 \times 10^{22}$ m^{-2} s^{-1} and energies corresponding to $kT_i \approx 200$ eV can be derived for the 90 kA discharges.

The asymmetry of the ion saturation current and the maximum in deuterium implantation and impurity deposition at the sides of the graphite probes can be explained by ion drift in the toroidal direction, either as a result of $E \times B$ drift due to the radial electric field, or as a diamagnetic drift. Recent measurements of drift motion in tokamak edge plasmas with the Gundestrup probe [12] were interpreted using a onedimensional fluid model. We choose to interpret the data by means of a particle model [2]. If we consider the case of particles with Maxwellian velocity distribution drifting leftwards in Fig. 1d with velocity $v = w\sqrt{2kT/m}$, then the flux density to the cylinder surface can be written:

$$\Gamma(\alpha) = n\sqrt{\frac{kT}{2\pi m}}\left[\exp(-w^2\cos^2\alpha) + \sqrt{\pi}\ \mathrm{erf}(-w\cos\alpha)w\cos\alpha\right]. \quad (1)$$

The solid contour in Fig. 7a shows the ratio $R(\alpha) \equiv \Gamma(\alpha)/\Gamma(\alpha - \pi)$ calculated from Eq. (1) using $w = 0.2$, which makes a good fit with the deuterium trapping distribution at $r = 58$ mm in a series of 40 kA shots. The deuterium trapping at $r = 53$ mm in a series of 90 kA shots also shows a large asymmetry in the same direction, a factor 8 corresponding to $w = 0.6$ as shown in Fig. 7b. A similar asymmetry is observed in the ion saturation current and in the impurity deposition. Thus there appears to be a toroidal drift at the edge, leftwards in Fig. 1d, i.e. in the direction of the toroidal current on axis. The edge magnetic field is close to poloidal and $B_\theta(a) \approx 0.2$ T in the 90 kA shots. From the estimates of the radial electric field then, a leftward drift of $E/B_\theta(a) \approx 22$ km/s is expected outside $r \approx 55$ mm, and a drift of ~ 7 km/s towards the right in the region $51 \leq r < 55$. However, from Fig. 7 there does not appear to be such a change of direction. The density gradient on the other hand is always directed

inwards, and consequently a leftward diamagnetic drift of order $v_d \approx kT_i/(eB\lambda_n)$ should be present, where λ_n is the scale length of the density gradient. Identifying the drift in Fig. 7b with a superposition of diamagnetic and $E \times B$ drift gives $T_i \approx 40$ eV, or $T_i/T_e \approx 2$.

From the passive probe measurements we conclude that there is a component of high energy ions and neutrals which hits the wall with a flux density of $(7\text{–}8) \times 10^{22}$ m^{-2} s^{-1}. The energies of these particles correspond to ion temperatures of $kT_i \approx 100$ eV in the 40 kA discharges and $kT_i \approx 200$ eV in the 90 kA shots. The sputtering yield of stainless steel by these particles in the deuterium case is $\sim 1\%$ and $\sim 2\%$ respectively [13], if we allow for a factor 2 enhancement due to non-normal incidence. This is in good agreement with the observed metal deposition rates.

There remains some ambiguity concerning the edge ion temperature. If $T_i \approx T_e$ is valid we can take $n_e(a) \approx 8 \times 10^{18}$ m^{-3} as a representative value which does not change so much with the plasma current.

Due to screening only few sputtered metal atoms are expected to penetrate into the central plasma. If atoms which are ionised within one gyro radius from the wall are assumed to return to the wall then only a fraction $\sim \exp(-\rho/\lambda_i)$ has a chance to enter the plasma, where $\lambda_i = v_0/(n_e(a)\langle\sigma_i v_e\rangle)$ is the ionisation length and v_0 is the velocity of the neutral atom. E.g. for 2 eV sputtered iron atoms $\rho \approx 7.6$ mm and $\lambda \approx 4.1$ mm, such that at least 85% of the sputtered atoms are screened and return immediately to the wall.

5. Conclusions

Edge profiles of parallel heat flux, electron temperature, probe floating potential and particle flux have been measured in RFP discharges in T1. An asymmetric heat flux in the edge can be understood as an effect suprathermal electrons. A perpendicular ion drift in the edge has been measured and is interpreted as a combination of $E \times B$ drift and diamagnetic drift. From passive probe measurements it can be inferred that a large fraction of the particles which hit the wall consist of ions with energies corresponding to $kT_i \approx 100$ eV in 40 kA discharges and $kT_i \approx 200$ eV in 90 kA shots. The flux of metals deposited on the wall is consistent with uniform sputtering by these high energy ions, but the sputtered metal atoms are almost completely screened from the main plasma.

References

[1] I. Gudowska, H. Bergsåker, K-D. Zastrow, P. Brunsell, J. Drake, B. Emmoth, G. Hellblom and P. Hörling, J. Nucl. Mater. 196–198 (1992) 332.
[2] H. Bergsåker, I. Gudowska, B. Emmoth and E. Tennfors, Proc. 19th Eur. Conf. Contr. Fusion. Plasma Phys., Innsbruck, 1992, part I, p. 607.
[3] A. Möller, H. Bergsåker, G. Hellblom, I. Gudowska, J. Brzozowski and B. Emmoth, Proc. 20th Eur. Conf. Contr. Fusion. Plasma Phys., Lisabon, 1993, part II, p. 471.
[4] V. Antoni, M. Bagatin and E. Martines, Plasma. Phys. Control. Fusion 34 (1992) 1639.
[5] H. Lin, G.X. Li, R.D. Bengtson et al., Rev. Sci. Instr. 63 (1992) 4611.
[6] Y. Yagi, T. Shimada, I. Hirota et al., J. Nucl. Mater. 162–164 (1989) 702.
[7] J.C. Ingraham, R.F. Ellis, J.N. Downing et al., Phys. Fluids B 2 (1990) 143.
[8] V. Antoni, M. Bagatin and E. Martines, Proc. 19th Eur. Conf. Control. Fusion Plasma. Phys., Innsbruck, 1992, part I, p. 631.
[9] P.C. Stangeby, in: Physics of Plasma-wall Interactions in Controlled Fusion Devices, D.E. Post and R. Behrisch, eds. (Plenum, 1986).
[10] G. Staudenmaier, J. Roth, R. Behrisch et al., J. Nucl. Mater. 84 (1979) 149.
[11] W.R. Wampler, D.K. Brice and C.W. Magee, J. Nucl. Mater. 102 (1981) 304.
[12] C.S. MacLatchy, C. Boucher, D.A. Poirier and J. Gunn, Rev. Sci. Instr. 63 (1992) 3923.
[13] J. Bohdansky, in: Data Compendium for Fusion, Nucl. Fusion special issue 1984, p. 61.